ADVANCES IN ATMOSPHERIC SCIENCES, VOL. 38, FEBRUARY 2021, 317–328

• Data Description Article •

BCC-ESM1 Model Datasets for the CMIP6 Aerosol Chemistry Model Intercomparison Project (AerChemMIP)

Jie ZHANG*[1], Tongwen WU[1], Fang ZHANG[1], Kalli FURTADO[2], Xiaoge XIN[1], Xueli SHI[1], Jianglong LI[1], Min CHU[1], Li ZHANG[1], Qianxia LIU[1], Jinghui Yan[1], Min WEI[3], and Qiang MA[3]

[1]*Beijing Climate Center*, *China Meteorological Administration*, *Beijing* 100081, *China*

[2]*Met Office Hadley Centre, Exeter* EX1 3PB, *UK*

[3]*National Meteorological Information Center*, *China Meteorological Administration*, *Beijing* 100081, *China*

(Received 23 May 2020; revised 28 September 2020; accepted 10 November 2020)

ABSTRACT

BCC-ESM1 is the first version of the Beijing Climate Center's Earth System Model, and is participating in phase 6 of the Coupled Model Intercomparison Project (CMIP6). The Aerosol Chemistry Model Intercomparison Project (AerChemMIP) is the only CMIP6-endorsed MIP in which BCC-ESM1 is involved. All AerChemMIP experiments in priority 1 and seven experiments in priorities 2 and 3 have been conducted. The DECK (Diagnostic, Evaluation and Characterization of Klima) and CMIP historical simulations have also been run as the entry card of CMIP6. The AerChemMIP outputs from BCC-ESM1 have been widely used in recent atmospheric chemistry studies. To facilitate the use of the BCC-ESM1 datasets, this study describes the experiment settings and summarizes the model outputs in detail. Preliminary evaluations of BCC-ESM1 are also presented, revealing that: the climate sensitivities of BCC-ESM1 are well within the likely ranges suggested by IPCC AR5; the spatial structures of annual mean surface air temperature and precipitation can be reasonably captured, despite some common precipitation biases as in CMIP5 and CMIP6 models; a spurious cooling bias from the 1960s to 1990s is evident in BCC-ESM1, as in most other ESMs; and the mean states of surface sulfate concentrations can also be reasonably reproduced, as well as their temporal evolution at regional scales. These datasets have been archived on the Earth System Grid Federation (ESGF) node for atmospheric chemistry studies.

Key words: BCC-ESM1, CMIP6, AerChemMIP, climate sensitivity, precipitation, surface air temperature, sulfate

Citation: Zhang, J., and Coauthors, 2021: BCC-ESM1 model datasets for the CMIP6 Aerosol Chemistry Model Intercomparison Project (AerChemMIP). *Adv. Atmos. Sci.*, **38**(2), 317−328, https://doi.org/10.1007/s00376-020-0151-2.

1. Introduction

Climate impacts of atmospheric chemistry, especially the contribution of tropospheric ozone precursors to radiative forcing, have been estimated in all the Intergovernmental Panel on Climate Change (IPCC) reports. However, even the models used in the IPCC's fourth report were mostly offline chemistry transport models, and none of the climate models included tropospheric ozone chemistry (Collins et al., 2017). The Atmospheric Chemistry and Climate Model Intercomparison Project (ACCMIP) was launched in 2011 and aimed to document changes in atmospheric composition and the associated radiative forcings in CMIP5 models (Lamarque et al., 2013). However, the model setups for ACCMIP were generally different from CMIP5 (with lower resolution but more complex chemistry) and only four of the models could be used to estimate future climate changes in surface ozone (Schnell et al., 2016). To build on the experiences of previous programs, the CMIP6-endorsed Aerosol Chemistry Model Intercomparison Project (AerChemMIP) is a series experiments with the goal of quantifying the effects of near-term climate forcers (NTCFs: methane, tropospheric aerosols and ozone, and their precursors) and reactive well-mixed greenhouse gases (WMGHGs) on climate and air quality (Collins et al., 2017). AerChemMIP is designed to answer four scientific questions: (1) how have anthropogenic emissions contributed to global radiative forcing and affected regional climate over the historical period? (2) How might future policies (on climate, air quality, and land use) affect the abundances of NTCFs and their climate impacts? (3) How do uncertainties in historical NTCF emissions affect radiative forcing estimates? (4) How important are climate feedbacks to natural NTCF emissions, atmospheric composition, and radiative effects?

BCC-ESM1 is a new version of the Beijing Climate Cen-

* Corresponding author: Jie ZHANG
Email: jiezhang@cma.gov.cn

ter's ESM that includes interactive atmospheric chemistry and aerosols. Its details are described in Wu et al. (2020a). BCC-ESM1, along with 14 other ESMs, have participated in AerChemMIP, including CESM2-WACCM, CNRM-ESM2-1, EC-Earth3-AerChem, EMAC-2-54-AerChem, GFDL-ESM4, GISS-E2.1, IPSL-CM5A2-INCA, IPSL-CM6A-AER-LR, MIROC6, MIROC-ES2L, MPI-ESM-1-2-HAM, MRI-ESM2-0, NorESM2, and UKESM1-0-LL. All of these ESMs are run in AerChemMIP and the other programs under CMIP6 [DECK (Diagnostic, Evaluation and Characterization of Klima) and the other CMIP6-endorsed MIPs] with their maximum available complexity. Therefore, their results can be shared across MIPs and used for more comprehensive assessments. The AerChemMIP experiments are classified into three tiers by their priority. The AerChemMIP is the first international MIP that BCC-ESM1 has been involved in, and thus far it has conducted all its Tier 1 experiments and seven experiments in lower priorities. BCC-ESM1 has also run the DECK and CMIP historical simulations, which serve as the "entry cards" for models participating in CMIP6 (Eyring et al., 2016).

AerChemMIP is the first chemistry program fully involved in the CMIP structure. Most of its experiments are newly designed and of special scientific interest. This paper introduces the experiment settings as well as the BCC-ESM1 outputs, to facilitate their use. Following this introduction, a brief overview of BCC-ESM1 is provided in section 2. The experiments run by BCC-ESM1 are also summarized in that section. Section 3 presents a technical validation of BCC-ESM1, including the model climate sensitivity and evaluations of surface air temperature (SAT), precipitation, and surface sulfate concentrations. Section 4 provides a summary, and section 5 shows some usage notes.

2. Model and experiments

2.1. *Model configuration*

BCC-ESM1 is based on the climate system model BCC-CSM2 (Wu et al., 2019a), but includes interactive representations of tropospheric chemistry and aerosols. As the successor of BCC-CSM1.1 (Wu et al., 2013), which participated in CMIP5, BCC-CSM2 included updates to the deep convection parameterization, considered the indirect effects of aerosols and gravity wave drag generated by deep convection, and introduced a new scheme for the cloud fraction. BCC-CSM2-MR, the medium resolution version of BCC-CSM2, shows an overall improvement in many aspects, such as the tropospheric air temperature at the global and regional scale in East Asia, the stratospheric quasi-biennial oscillation, and the Madden–Julian Oscillation.

The atmospheric component of BCC-ESM1 is BCC-AGCM3-Chem (Wu et al., 2020a), which includes an interactive tropospheric gas-phase and aerosol chemistry scheme. The model includes 66 gas-phase species and 13 prognostic aerosol species. The main atmospheric chemistry built in BCC-AGCM3-chem is based on MOZART2 (Model for OZone And Related chemical Tracers, version 2), a troposphere-only chemistry transport model developed by the National Center for Atmospheric Research (Horowitz et al., 2003). SO_2, dimethyl sulfide (DMS), and NH_3 are the gas tracers newly added to BCC-ESM1. A bulk aerosol scheme is also newly introduced in BCC-ESM1, including the relative reactions, transport, emissions, and depositions. The aerosol species involved are sulfate (SO_4^{2-}), hydrophobic and hydrophilic organic carbon (OC1 and OC2), hydrophobic and hydrophilic black carbon (BC1 and BC2), four categories of soil dust (DST01, DST02, DST03, DST04), and four categories of sea salt (SSLT01, SSLT02, SSLT03, SSLT04). Dust and sea salt aerosols are classified into four size bins by diameter. The mass-mixing ratios of each aerosol type are prognostic variables. Prognostic aerosol masses are used to estimate the liquid cloud droplet number concentration and the indirect effects of aerosols are considered.

To save computing resources and tune the model more efficiently, BCC-AGCM3-Chem has a relatively low horizontal resolution of T42 (about 280 km) and has 26 vertical levels with the top level at 2.914 hPa. The land component of BCC-ESM1 is the BCC Atmosphere and Vegetation Interaction Model, BCC-AVIM2.0, with terrestrial carbon cycle (Li et al., 2019). The oceanic component is the Modular Ocean Model, version 4, with 40 levels included (MOM4-L40; Griffies et al., 2005). The sea-ice component is the Sea Ice Simulator (SIS), with three vertical layers, one snow cover layer, and two ice layers (Winton, 2000). MOM4-L40 and SIS use a tripolar grid with a horizontal resolution of 1° longitude by 1/3° latitude between 10°S and 10°N, increasing to 1° at 30°S and 30°N.

2.2. *Experiments*

The experiments conducted by BCC-ESM1 are summarized in Table 1. The simulation data have been archived on the Earth System Grid Federation (ESGF) node (https://esgf-node.llnl.gov/projects/cmip6/). DECK includes four basic experiments: (a) a historical Atmospheric Model Intercomparison Project (*amip*) simulation; (b) a control simulation under pre-industrial conditions (*piControl*); (c) a simulation that branches from *piControl* in 1850 and is forced by an abruptly quadrupled global-mean concentration of CO_2 (*abrupt-4×CO2*); and (d) a simulation that branches from *piControl* and is forced by a gradually increased CO_2 concentration at a rate of 1% per year (*1pctCO2*). *Amip* is run by an atmospheric general circulation model (AGCM) with prescribed sea surface temperature (SST) and sea-ice concentration (SIC) and include three ensemble members. The other three experiments are all conducted by a coupled atmosphere–ocean general circulation model (AOGCM) and include only one ensemble member. The CMIP historical experiment (*historical*) is also conducted by the AOGCM. It branches from *piControl* and is forced by evolving external forcing. There are three ensemble members for *historical* with slightly varying initial conditions. *Amip*, *piControl,*

Table 1. Experiments conducted by BCC-ESM1.

	Experiment ID	Integration Time	Model Configuration	Experiment design	Member number
DECK	*amip*	1979–2014	AGCM	Performed under the evolving, externally imposed forcings and boundary conditions (SST and SIC) downloaded from the CMIP6 website.	3
	piControl	1850–2300	AOGCM	Performed under conditions in the year 1850. The integration starts from the model state after 400 years of spin-up.	1
	abrupt-4×CO2	1850–2000	AOGCM	Branched from *piControl* and forced under an abrupt quadrupling of the CO_2 concentration in 1850, then held fixed at this level. Other forcings are all fixed at their 1850 values.	1
	1pctCO2	1850–2000	AOGCM	Branched from *piControl* and forced under a gradually increased CO_2 concentration at a rate of 1% per year. Other forcings are all fixed at their 1850 values.	1
CMIP historical	*historical*	1850–2014	AOGCM	Branched from *piControl* and forced by evolving, externally imposed forcings.	3
AerChemMIP (Tier-1)	*hist-piNTCF*	1850–2014	AOGCM	Parallels *historical* with all forcings applied, but fixed anthropogenic emissions of aerosol and ozone precursors to their 1850 values.	3
	ssp370	2015–2055	AOGCM	Transient future projection branched from *historical*, following the SSP3-7.0 scenarios for WMGHG and NTCF emissions.	3
	ssp370-lowNTCF	2015–2055	AOGCM	Same as *ssp370*, but following the SSP3-7.0-lowNTCF scenarios.	3
	piClim-control	1850–1880	AGCM	Performed under 1850 concentrations of WMGHGs and emissions of NTCFs with SST and SIC prescribed as a (monthly varying) climatology taken from 30 years of *piControl*.	1
	piClim-NTCF	1850–1880	AGCM	Same as *piClim-control*, but with the emissions of aerosol and ozone precursors set to present-day (2014) values.	1
	piClim-CH4	1850–1880	AGCM	Same as *piClim-control*, but with the CH_4 concentration set to present-day (2014) values.	1
	histSST	1850–2014	AGCM	Branched from *piClim-control* with prescribed SST and SIC. The SST and SIC are specified as the monthly mean time-evolving values from *historical*. All forcing is the same as *historical*.	1
	histSST-piNTCF	1850–2014	AGCM	Same as *histSST*, but fixed anthropogenic emissions of aerosol and ozone precursors to their 1850 values.	1
	histSST-piCH4	1850–2014	AGCM	Same as *histSST*, but fixed CH_4 concentrations to their 1850 values.	1
	ssp370SST	2015–2055	AGCM	Branched from *amip* with prescribed SST and SIC from *ssp370*. All forcings are the same as *ssp370*.	1
	ssp370SST-lowNTCF	2015–2055	AGCM	Branched from *amip* with prescribed SST and SIC from *ssp370-lowNTCF*. All forcings are the same as *ssp370-lowNTCF*.	1
AerChemMIP (Tier-2)	*hist-piAer*	1850–2014	AOGCM	Parallels *historical* with all forcings applied, but fixed anthropogenic emissions of aerosol precursors to their 1850 values.	3
	piClim-aer	1850–1880	AGCM	Same as *piClim-control*, but with the emissions of aerosol precursors set to present-day (2014) values.	1
	piClim-BC	1850–1880	AGCM	Same as *piClim-control*, but with the emissions of black carbon precursors set to present-day (2014) values.	1
	piClim-O3	1850–1880	AGCM	Same as *piClim-control*, but with the emissions of ozone precursors set to present-day (2014) values.	1
AerChemMIP (Tier-3)	*piClim-NOX*	1850–1880	AGCM	Same as *piClim-control*, but with the emissions of NO_x set to present-day (2014) values.	1
	piClim-VOC	1850–1880	AGCM	Same as *piClim-control*, but with the emissions of CO and VOCs set to present-day (2014) values.	1
	piClim-SO2	1850–1880	AGCM	Same as *piClim-control*, but with the emissions of SO_2 set to present-day (2014) values.	1

and *historical* are baselines for many CMIP6-Endorsed MIPs. *Abrupt-4×CO2* and *1pctCO2* are used to estimate model climate sensitivities and feedbacks.

The AerChemMIP experiments are run with the same complexity as in DECK and *historical*. The experiments are classified into three tiers by their priority. The Tier 1 experi-

ments mainly focus on the impacts of NTCFs and reactive well-mixed gases on historical and future climate, as well as future NTCFs under different air quality policies. Tier 2 and 3 will examine the effects of NTCF emissions and climate feedback more specifically, to provide detailed uncertainty estimates.

BCC-ESM1 has run all the Tier 1 experiments and seven Tier 2 and 3 experiments:

- *hist-piNTCF* in Tier 1 parallels *historical* but with the anthropogenic emissions of aerosols, and ozone precursors fixed to their 1850 values. *hist-piAer* in Tier 3 is similar to *hist-piNTCF* but with the anthropogenic emissions of aerosol fixed to the 1850 values. By comparing with *historical*, these experiments can be used to estimate the climate impacts of anthropogenic emissions of NTCFs and aerosols. Three ensemble members are conducted for both *hist-piNTCF* and *hist-piAer* with the same initial conditions as *historical*.
- *piClim-control* in Tier 1 is run under pre-industrial conditions for 31 years with prescribed SST and SIC from 30 years of *piControl* climatology. It is designed following the protocols of the Radiative Forcing Model Intercomparison Project (Pincus et al., 2016). Eight more *piClim-X* experiments are also conducted by BCC-ESM1 that branch from *piClim-control*: (a) *piClim-NTCF* and *piClim-CH4* in Tier 1, which are the same as *piClim-control* but set NTCF emissions and the CH_4 concentration to present-day values, respectively; (b) *piClim-aer*, *piClim-BC* and *piClim-O3* in Tier 2, which set the emissions of aerosol precursors, black carbon and ozone precursors to present-day values, respectively; (c) *piClim-NOX*, *piClim-VOC* and *piClim-SO2* in Tier 3, which set the NOx, CO and VOCs, and SO_2 emissions to present-day values, respectively. These experiments can help to quantify the effective radiative forcings (ERFs) at pre-industrial levels due to different drivers, as in Thornhill et al. (2020). The *piClim-X* experiments include only one ensemble per experiment in BCC-ESM1.
- *histSST* in Tier 1 also branches from *piClim-control* but with prescribed time-evolving SST and SIC from *historical*. All other forcings are the same as in *historical*. *histSST-piNTCF* and *histSST-piCH4* in Tier 1 are the same as *histSST* and branch from the same point as *histSST* but with the NTCF precursors and methane fixed to their 1850 values, respectively. These experiments can help to diagnose the transient ERFs for NTCF and methane. The *histSST-X* experiments include only one ensemble per experiment.
- *ssp370* in Tier 1 is a future simulation with the highest levels of short-lived climate pollutants without climate policy. It achieves forcing levels of 7.0 W m^{-2} in 2100. *ssp370-lowNTCF* in Tier 1 is a future simulation with strong levels of air quality control measures. Both experiments branch from the *historical* experiments in 2015 and are run for 50 years from 2015 to 2055 instead of 85 years from 2015 to 2100 as suggested by AerChemMIP, to reduce the computational expense. These experiments can help to estimate the impacts on future climate and air quality, as in Allen et al. (2020) and Turnock et al. (2020). Three ensemble members are conducted for both *ssp370* and *ssp370-lowNTCF*.
- *ssp370SST* in Tier 1 is a transient future prescribed-SST simulation following the ssp370 scenario. It branches from the first member of *amip* in year 2015 with prescribed SST and SIC from the first member of the *ssp370* experiment. *ssp370SST-lowNTCF* in Tier 1 branches at the same point as *ssp370SST* with prescribed SST and SIC from the first member of *ssp370-lowNTCF* following the *ssp370-lowNTCF* scenario. Different ERF changes between these future prescribed SST simulations and the relevant coupled model projections (*ssp370* and *ssp370-lowNTCF*) help to quantify the efficacy of NTCFs to affect climate. Both experiments include only one ensemble.

3. Technical validation

3.1. *Model climate sensitivities to idealized CO_2 forcing*

Climate sensitivity is an important metric for model evaluation. It is one of the major factors responsible for different model climate responses and uncertainty in future climate projections (Grose et al., 2018). Here, we estimate the global mean SAT response to idealized CO_2 forcing by using the *1pctCO2* and *abrupt-4×CO2* experiments. Both experiments are initialized from the *piControl* experiment, which is used as the reference experiment.

The transient climate response (TCR) is calculated from the *1pctCO2* simulation in which CO_2 is gradually increased at a rate of 1% per year. The TCR is defined as the annual mean SAT change relative to the *piControl* equilibrium climate state, averaged over a 20-year period centered on the time at which the CO_2 concentration was doubled (year 70 of the simulation). The *1pctCO2* forcing resembles the CO_2 forcing in the 21st century but is more idealized. As shown in Fig. 1a, the evolution of SAT anomaly is linearly correlated with the CO_2 concentration in the *1pctCO2* experiment. A high linear correlation is also evident in observations at both global and regional scales (Wu et al., 2019b). The TCR in BCC-ESM1 is about 1.78 K, which is 1.40 K for BCC-CSM2-MR (Shi et al., 2020). The TCRs in both BCC models lie within the "likely" range of 1.0–2.5 K suggested by IPCC AR5 (Bindoff et al., 2013). In the *1pctCO2* experiment and the real world, the distribution of heat flux at the atmosphere–ocean interface has not yet reached equilibrium.

The equilibrium climate sensitivity (ECS) is measured as the SAT changes in a double CO_2 experiment when the cli-

mate system reaches its equilibrium climate state. The ECS in BCC-ESM1 is estimated by the *abrupt-4xCO2* experiment. SAT changes in the *abrupt-4xCO2* experiment are shown in Fig. 1b. The model response to quadrupled CO_2 can be separated into a fast-response stage in the first two decades and a slow-response stage afterward. Following the approach of Gregory et al. (2004), we regress the global annual mean net radiative-flux changes at the top of the atmosphere (TOA) on SAT changes and then extrapolate to zero net flux (Fig. 2). The ECS is then defined as half of the *x*-intercept concerning a CO_2 doubling. This method yields an ECS estimate of 3.34 K for BCC-ESM1, which is 3.03 K for BCC-CSM2-MR (Wu et al., 2019a). ECSs in both BCC-ESM1 and BCC-CSM2-MR are within the "likely" range of 1.5–4.5 K suggested by IPCC AR5.

3.2. *SAT in piControl and historical experiments*

Figure 3a shows the evolution of the global mean annual averaged SAT in the *piControl* run. In *piControl*, SAT reaches a quasi-equilibrium state with a slight increasing trend of about 0.016°C (100 yr)$^{-1}$, which is much smaller than the standard deviation of SAT (0.10°C yr^{-1}). Time series of annual mean SAT anomalies from the three members of the CMIP6 historical simulations are shown in Fig. 3b, as well as the observation from HadCRUT4 (https://www.metoffice.gov.uk/hadobs/hadcrut4/). The anomalies are relative to the 1850–1950 mean. The SAT simulations show good agreement with HadCRUT in the first 100 years. However, there is a significant cooling bias in the second half of the 20th century, especially over the period from the 1960s to 1990s. We colloquially refer to this significant cooling bias as the "pot-hole" bias (because it represents an undesirable dip in the "road" of an accurately simulated SAT trend). It is a common problem in most of the ESMs participating in CMIP6. One possible reason for the pot-hole bias is that the prognostic aerosol schemes produce overly strong aerosol cooling (Flynn and Mauritsen, 2020; Meehl et al., 2020).

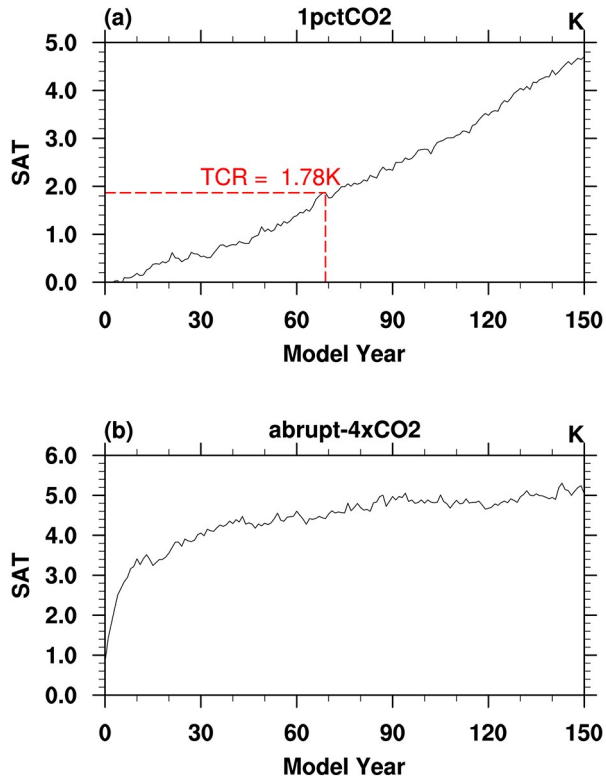

Fig. 1. (a) Temporal evolution of globally averaged SAT changes relative to the reference experiment (*piControl*) for the 151 model years in the *1%CO2* experiment. (b) As in (a) but for SAT changes in the *abrupt-4×CO2* experiment. Units: K.

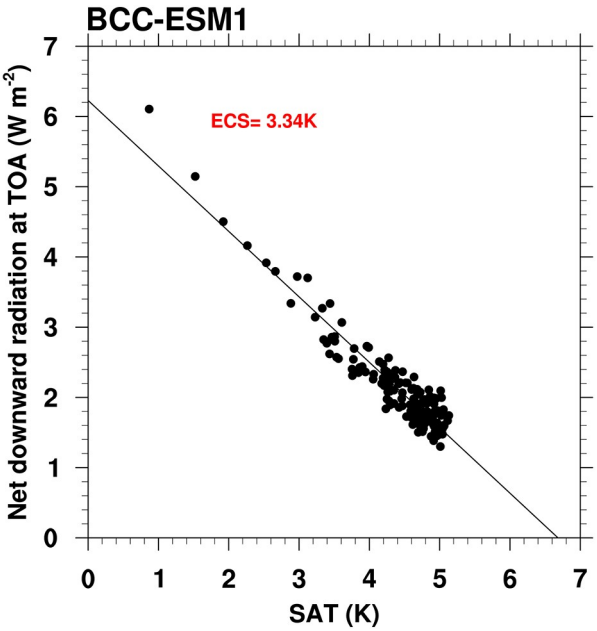

Fig. 2. Annual changes of the net TOA radiative flux and the global-mean SAT for the first 151 years of the abrupt CO_2 quadrupling experiment (*abrupt-4×CO2*) relative to the pre-industrial control run (*piControl*). The regression line is also calculated to estimate the ECS of BCC-ESM1.

The spatial structure of SAT in the *historical* experiment is examined over the period from 1986 to 2005 (Fig. 4), as well as its biases compared with ERA5 reanalysis (Copernicus Climate Change Service, 2017). The spatial structure of SAT is well captured with a spatial correlation of 0.99. Simulated SAT is about 0.35 K higher than that in ERA5, attributable to the warmer tropics and subtropics. Generally, the biases in BCC-ESM1 show great similarity with those in BCC-CSM2-MR (Wu et al., 2019a), including the slight systematic warm biases over oceans, as well as the relatively large warming/cooling biases over the polar regions. The biases over the oceans and polar regions may partly come from the ocean and sea-ice modules, which are the same in BCC-ESM1 and BCC-CSM2-MR. Both models also show systematic cool biases over most land regions. The cooling bias may be partly attributable to the land surface modeling component, since it is also evident in AMIP simulations, or to other processes like errors in cloud properties. The cooling biases in BCC-ESM1 may also be related to the overestimated sulfate concentration in the atmosphere shown in subsec-

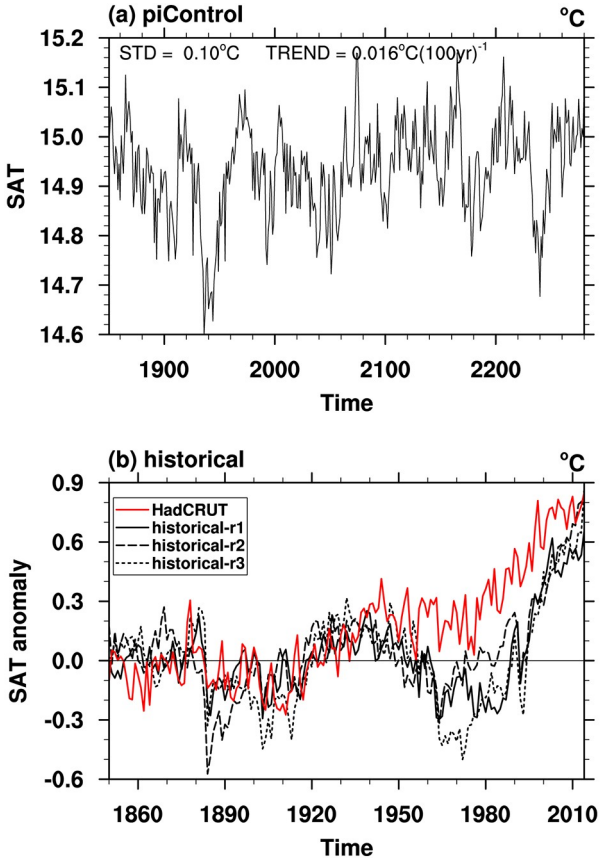

Fig. 3. (a) Time series of the global mean SAT in the *piControl* simulation. (b) Time series of the global mean SAT anomalies in the *historical* simulations (three members, black lines) and the observation (red line) from HadCRUT4. The anomalies are relative to the 1850–1950 mean.

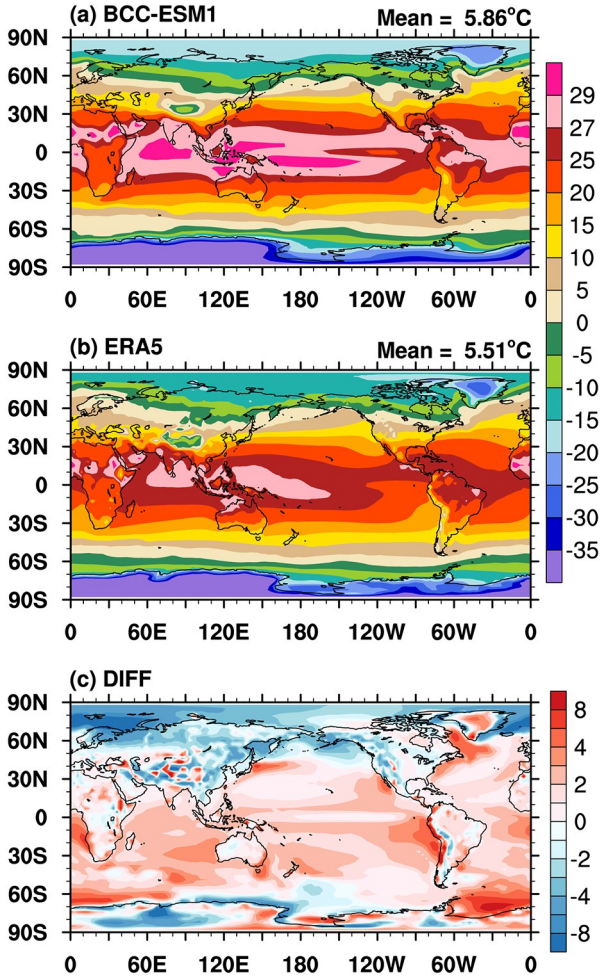

Fig. 4. Annual mean SAT in (a) BCC-ESM1 and (b) ERA5 reanalysis from 1986 to 2005. (c) The SAT biases. Units: °C.

tion 3.4.

3.3. *Precipitation and associated near-surface horizontal wind*

Annual mean precipitation in the *historical* experiment and its comparison with GPCP observation (Adler et al., 2003) are examined and shown in Fig. 5. The biases are generally within 1 mm d^{-1} and the global mean precipitation in BCC-ESM1 is very close to the observation: 2.27 mm d^{-1} versus 2.24 mm d^{-1}. BCC-ESM1 still suffers from the double ITCZ problem: precipitation south of the equator in the eastern Pacific is overestimated and the SPCZ is too zonally elongated. Zhang et al. (2015) found that the double ITCZ related biases include sufficient precipitation in the southeastern Pacific, warmer SST, weaker easterly flow, and stronger meridional wind divergences away from the equator. However, no progress can be identified from the multimodel ensemble (MME) mean in CMIP3 to that in CMIP5.

The double ITCZ measures are also examined for BCC-ESM1, as in Zhang et al. (2015). The SST bias in BCC-ESM1 closely resembles the SAT bias (not shown). As indicated by Fig. 4c, the warmer SST south of the equator amplifies the precipitation over the Southeast Pacific and leads to the eastward-extended SPCZ. Over the eastern tropical Pacific, the near-surface zonal wind weakens and the meridional wind converges south of the equator (Fig. 6). Both zonal and meridional wind biases contribute to the SPCZ biases in BCC-ESM1. Generally, biases of the double ITCZ measures in BCC-ESM1 are quite similar to those in the CMIP3 and CMIP5 MMEs. With great improvements in atmospheric physical parameterizations, the double ITCZ bias is much weaker in the newly developed high-resolution climate system model, BCC-CSM3-HR (Wu, 2020b).

Other model deficiencies in precipitation reproductions are evident, including the overestimations over eastern Indonesia, western Indian Ocean, southern Africa, and East Asia. Meanwhile, underestimations are pronounced north of the equator in the Pacific and Atlantic. Such biases seem to be common in CMIP3 and CMIP5 models (Oueslati and Bellon, 2015). The sufficient precipitation over eastern Indonesia and the western Indian Ocean accompanies stronger trade winds in the east. The anomalous easterlies converge toward the biased precipitation, west of the Maritime Continent and the eastern African coast. The underestimations north of the equator in the Pacific and Atlantic are asymmet-

ric with the overestimations in the south, which may be attributable to the asymmetric warming amplitudes by the equator as well as the local meridional wind divergences (Zhang et al., 2015). The Southern Africa and East Asia are greatly affected by the global monsoon system, and the precipitation biases can be related to many physical and dynamic processes, but investigating these is beyond the scope of the present study.

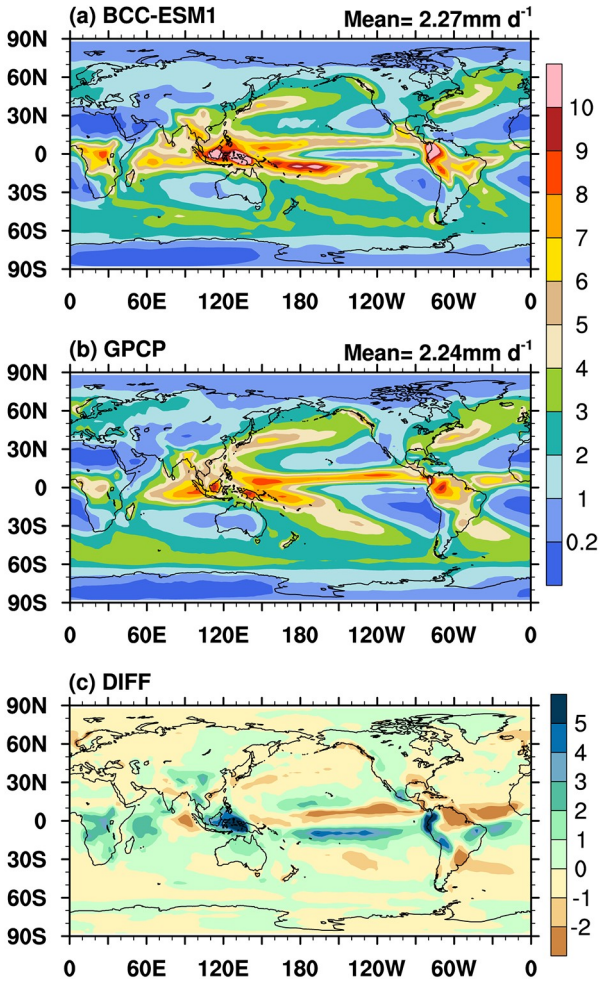

Fig. 5. Annual mean precipitation in (a) BCC-ESM1 and (b) GPCP from 1986 to 2005. (c) The precipitation biases. Units: mm d^{-1}.

3.4. *Surface sulfate and its variation*

Sulfate is a major species of aerosol. Sulfate aerosols can cool the atmosphere by reflecting solar irradiation directly or by making clouds more reflective via aerosol indirect effects. The anthropogenic emissions of SO_2 from fuel combustion and industrial activities constitute the main precursor of atmospheric sulfate. A large amount of sulfate in the atmosphere is believed to have significant cooling effects at regional and global scales, although large uncertainties remain in the magnitude of these effects. BCC-ESM1 can capture the major features of aerosols reasonably well in comparison with observed aerosol concentrations and their optical properties (Wu et al., 2020a). In this paper, we use ground-based monitoring networks to extend the evaluation of sulfate. Simulation from the historical experiment is examined here.

The sulfate observations are from three monitoring networks: the European Monitoring and Evaluation Program (EMEP; Tørseth et al., 2012); the United States Interagency Monitoring of Protected Visual Environment (IMPROVE; Malm et al., 2004) extensive ground-based networks; and the Acid Deposition Monitoring Network in East Asia (EANET, 2019). For each observation site, model data are selected only when the monthly observation is available. To maximize the amount of data available for comparison but also ensure the climatological representativeness of the observation, all 12 monthly means are required to calculate an annual mean, as in Mulcahy et al. (2020).

The annual mean surface sulfate concentrations from 274 monitoring sites are calculated and shown in Fig. 7a. Surface sulfate concentrations at EMAP, EANET and IMPROVE sites are about 3.33 μg m^{-3}, 3.20 μg m^{-3} and 1.35 μg m^{-3}, respectively. Generally, sulfate is higher in southern Europe than in northern Europe and higher in the

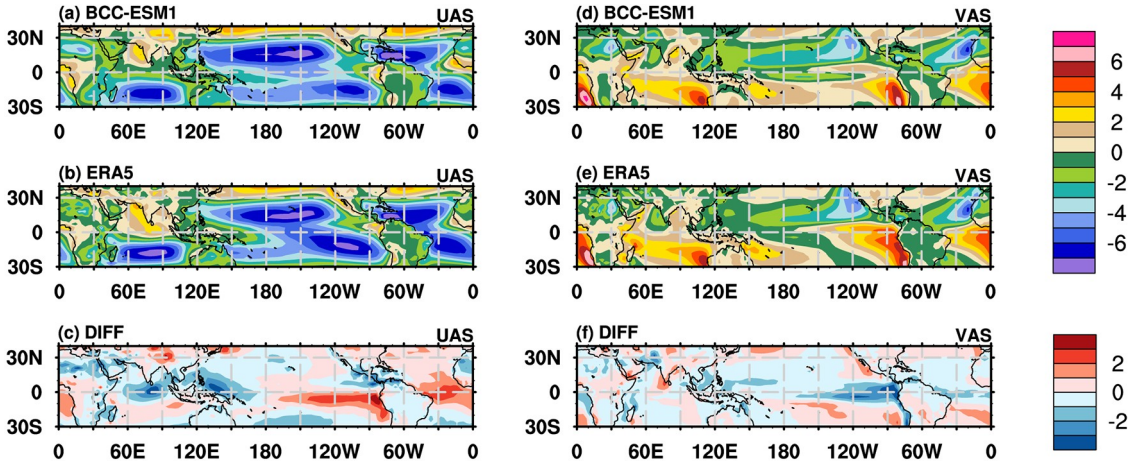

Fig. 6. Annual mean near-surface zonal wind (UAS) in (a) BCC-ESM1 and (b) ERA5 from 1986 to 2005. (c) The UAS biases. (d–f) As in (a–c) but for the near-surface meridional wind (VAS). Units: m s^{-1}.

east of the U.S. than in the west. BCC-ESM1 tends to overestimate the observations by about 0.95 μg m^{-3} but shows a high spatial correlation of 0.77, significant at the 1% level using a Student's *t*-test (Fig. 7b). The surface sulfate concentrations are comparable with the observation at the EMEP sites (3.18 μg m^{-3}) but overestimated by approximately 2 μg m^{-3} at the EANET and IMPROVE sites. BCC-ESM1 can capture the observed sulfate centers well over the eastern U.S., southern Europe, and Japan.

Regional statistical evaluations are shown in Fig. 8. Considering the relatively low model resolution and the high heterogeneous distribution of sulfate, simulations falling with the range of 50% to 200% of the observations (gray dashed lines in Fig. 8) are considered to be reasonable. Over the EMEP sites (Europe), the model shows a significant correlation of 0.66, with a slight underestimation over the southern EMEP sites, where the measured sulfate concentration is relatively large. Over EANET sites (East Asia), the comparison shows a high degree of scattering, with a low correlation with the observation of 0.39. Over the western U.S., the sulfate concentration is about twice that of the observation. As one of the major emission centers, the eastern U.S. is more polluted than the west. Among the four regions, the simulations perform best over the eastern U.S., with the highest correlation coefficient with the observation (0.87) and the smallest root-mean-square error (RMSE; 1.04 μg m^{-3}). Generally, the performance of BCC-ESM1 in reproducing the surface sulfate concentration is comparable to instrumental measurements, and its performance is comparable with that of UKESM1 (Mulcahy et al., 2020). The major discrepancy is that BCC-ESM1 tends to overestimate sulfate levels over the western U.S. and East Asia, which may partly contrib-

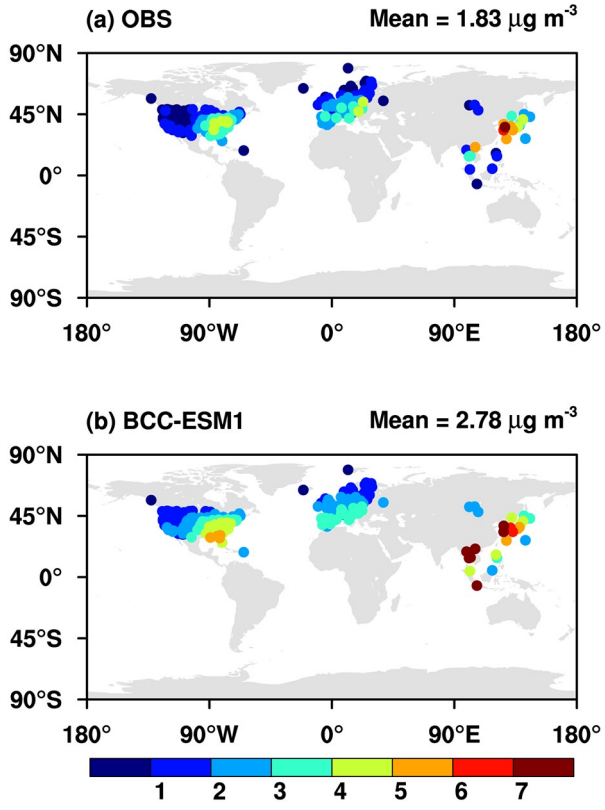

Fig. 7. (a) Annual mean surface sulfate concentration in 2000–09 at 274 monitoring sites in the three ground-based networks: EMEP in Europe, IMPROVE in the U.S., and EANET in East Asia. (b) Corresponding simulation in BCC-ESM1. All 12 monthly means are required to calculate annual mean results. Units: μg m^{-3}.

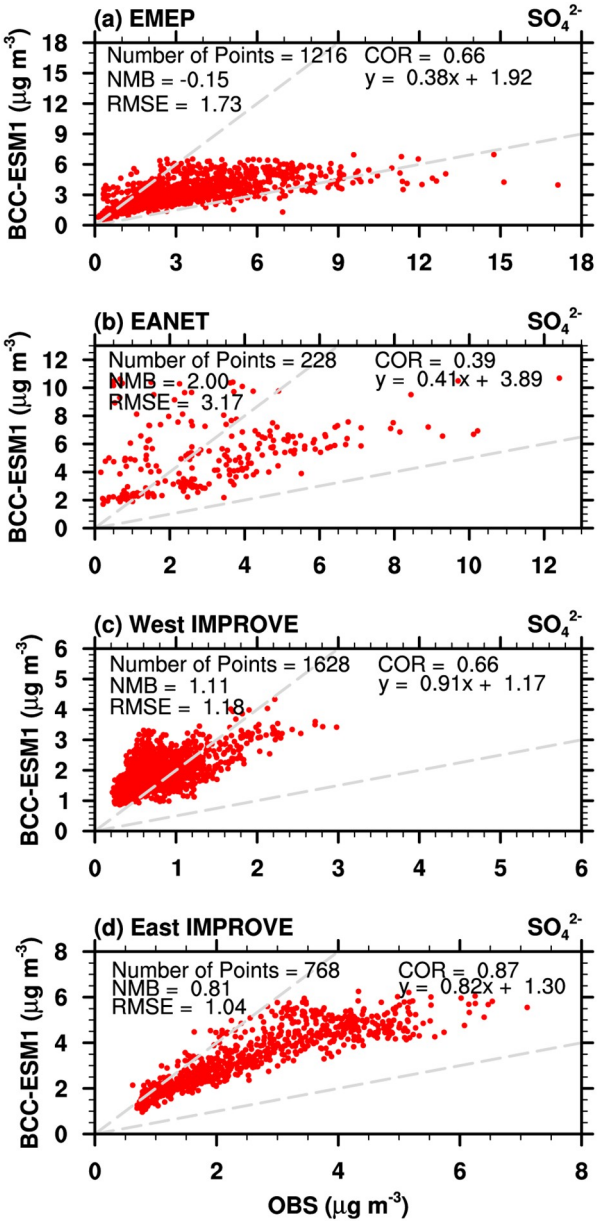

Fig. 8. Comparison of simulated annual mean SO_4^{2-} from BCC-ESM1 against ground-based measurements from (a) EMEP (Europe), (b) EANET (East Asia), (c) West IMPROVE (western U.S.), and (d) East IMPROVE (eastern U.S.) networks. Observations and model data cover the years 1978 to 2009 for EMEP, 2000 to 2014 for EANET, and 1990 to 2014 for IMPROVE. NMB stands for normalized mean bias, RMSE for root-mean-square error, and COR for correlation coefficient. Linear regression statistics are also included. Units: μg m^{-3}.

ute to the regional cooling biases as shown in Fig. 4c.

Figure 9 shows the evolution of the simulated and observed annual mean sulfate concentration, averaged across all the available ground-based observations, for all available years in the four typical regions. The uncertainty is calculated as ±1 standard deviation of the observed annual means across all the measurement sites. Simulations are suggested to be comparable with observations if the evolutions of the mean series of all sites are similar and the bands of uncertainty ranges are well overlapped. Generally, despite the systematic overestimation in East Asia and the western U.S., BCC-ESM1 can reproduce the changes in sulfate concentration at regional scales reasonably well.

Over Europe (EMEP), the sulfate concentration decreases by about 4 μg m^{-3} from 1978 to 2009. BCC-ESM1 captures the reduction and the changes are well within the observed uncertainty range, albeit the negative trend is slightly smaller. This underestimation of the annual mean surface sulfate concentration over Europe is also evident in UKESM1 simulations (Mulcahy et al., 2020) and is suggested to be related to a low bias in wintertime in UKESM1 (Turnock et al., 2015).

Over EANET sites, the surface sulfate concentration increases slightly with large interannual variability and uncertainties (about 3–4 μg m^{-3}). It increases in the early 2000s, decreases by about 1.5 μg m^{-3} from 2006 to 2012, and then bounces back afterward. The model generally tracks the observation quite well, despite a systematic overestimation by about 2 μg m^{-3}. The simulation also shows large variations across all the measurement locations. Note that the EANET sites here are mostly in Japan and the southern countries. China is also a main sulfate emissions center with large spatial heterogeneity. Local evaluation over China will be interesting when high coverage monitoring data are available.

Over the western U.S., the sulfate concentration is relatively small with little to no trend. The simulated sulfate con-

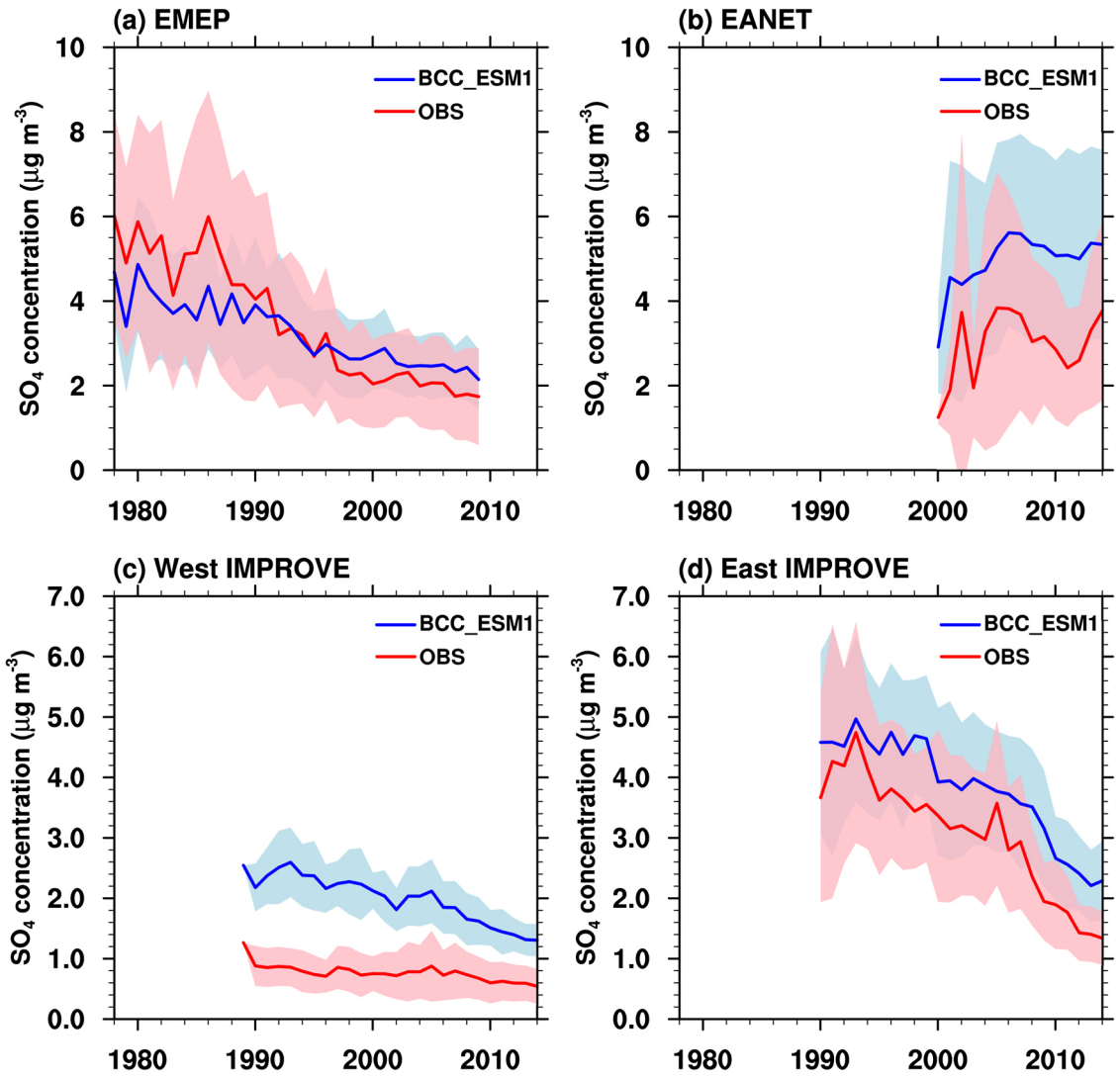

Fig. 9. Time series of annual mean observed (red lines) and simulated (blue lines) sulfate concentrations averaged across all measurement locations in each network for a particular year. Shaded areas show ±1 standard deviation of the observed and modeled annual mean values across all the measurement locations. Units: μg m^{-3}.

centration is about twice that of the observation with a small decreasing trend. This region is generally remote from source regions and differences may be attributable to the biases in transportation from the source region, oxidants, or removal rates (Mulcahy et al., 2020).

Over the eastern U.S., one of the major anthropogenic source regions, a significant negative trend is observed due to reductions in emissions. Although the model generally overestimates concentrations by about 0.8 $\mu g\ m^{-3}$, the decreasing rate and the uncertainty range in BCC-ESM1 show reasonable agreement with the observations.

4. Summary and relevant studies

This paper summarizes the experiments and datasets of BCC-ESM1, specifically for the CMIP6-endorsed AerChemMIP. The basic performance of BCC-ESM1 is evaluated, revealing that: the climate sensitivities in BCC-ESM1 are well within the likely ranges suggested by IPCC AR5; SAT and precipitation can be reasonably represented (the biases of which are discussed); and the present-day surface sulfate concentrations also compare well with observations, including their spatial structure and regional trends.

BCC-ESM1 is one of the few ESMs participating in CMIP6 with interactive atmospheric chemistry, and its AerChemMIP outputs have been widely used in recent atmospheric chemistry studies (i.e., Allen et al., 2020; Griffiths et al., 2020; Thornhill et al., 2020; Turnock et al., 2020). For example, in the special issue for AerChemMIP, BCC-ESM1 data are used to estimate the climate and air quality impact of mitigation policies. Turnock et al. (2020) used the outputs from BCC-ESM1 and nine other ESMs to make a first assessment of the impact on historical and future changes to air pollutants (O_3 and $PM_{2.5}$). CMIP6 models show a consistent overestimation of surface O_3 concentration but an underestimation of surface $PM_{2.5}$ with a large diversity in the historical period. For scenario ssp370, which encompasses the highest levels of short-lived climate pollutants without climate policy, both surface O_3 and $PM_{2.5}$ increase across most regions. In BCC-ESM1, surface O_3 changes are about 3 ppbv higher than the multimodel mean value for the historical period and the surface O_3 prediction is large in scenario ssp370. The large O_3 response in BCC-ESM1 may be related to the absence of NO_x titration, which will reduce surface O_3 concentrations. Allen et al. (2020) quantified the 2015–2055 climate and air quality effects of non-methane NTCFs with "weak" and "strong" levels of air quality controls. Their findings suggest air quality improvement with non-methane NTCF reductions, but additional surface warming and wetting may occur, particularly in Asia and the Arctic. Generally, results in BCC-ESM1 are consistent with the seven other ESMs participating in CMIP6, both in terms of global mean climate anomalies and air pollution anomalies due to NTCF mitigation.

5. Usage notes

The variables of Priority 1 in AerChemMIP have been generated, including meteorological variables at various time scales (monthly, daily, six-hourly, and hourly) and chemical variable outputs at the monthly scale. All the variables are listed at http://clipc-services.ceda.ac.uk/dreq/tabs03/expt_AerChemMIP_AerChemMIP_1_1.html. For brevity, we summarize the chemical outputs in Table 2, including the volume mixing ratios of gas-phase chemical species in the atmosphere, the mass mixing ratios of aerosols, atmospheric optical thickness, etc.

The horizontal resolution of all the variables is T42 (approximately 280 km). Most of the 3D atmospheric outputs are on model atmosphere levels (26 levels in a hybrid sigma-pressure vertical coordinate system). To facilitate multimodel comparisons, 11 atmospheric variables are interpolated to 19 fixed pressure levels for monthly outputs, and 6 of them are interpolated to 8 fixed pressure levels for daily outputs (Table 3).

Acknowledgements. This work was jointly supported by the National Key Research and Development Program of China (Grant No. 2016YFA0602103), the National Key Research and Development Program of China CERC-WET Project (Grant No. 2018YFE0196000) and the National Natural Science Foundation of China (Grant No. 41805063).

Table 2. Chemical outputs of BCC-ESM1 in CMIP6. Variables marked with an asterisk (*) are only provided for the first member of historical experiments.

Output name	Description	Frequency
c2h6, c3h6, c3h8, ch3coch3, ch4, co, co2, dms, h2o, hcho, hno3, isop, n2o, no, no2, o3, oh, pan, so2	Volume mixing ratio of corresponding species	Monthly
lossch4,lossco, lossn2o	Monthly loss of atmospheric methane, carbon monoxide, and nitrous oxide	Monthly
mmrbc, mmrdust, mmroa, mmrso4, mmrss	Mass mixing ratio of elemental carbon, dust, organic aerosol, sulfate, and sea salt	Monthly
od550aer, od550dust, od550so4, od550ss	Atmosphere optical thickness at 550 nm of total aerosol, dust, sulfate, and sea salt	Monthly
cdnc	Cloud liquid droplet number concentration	Monthly
emilnox	Layer-integrated lightning production of NO_x	Monthly
jno2	Photolysis rate of NO_2	Monthly

Table 2. (Continued.)

Output name	Description	Frequency
o3loss	O_3 destruction rate	Monthly
o3prod	O_3 production rate	Monthly
o3ste	Ozone tracer intended to map out stratosphere–troposphere exchange of ozone	Monthly
photo1d	Photolysis rate of O_3 to O1d	Monthly
airmass*	Vertically integrated mass content of air in layer	Monthly
dryso2*	Dry deposition rate of SO_2	Monthly
wetso2*	Wet deposition rate of SO_2	Monthly
dryso4*	Dry deposition rate of SO_4	Monthly
wetso4*	Wet deposition rate of SO_4	Monthly

Table 3. Monthly outputs of 11 variables that have been interpolated to 19 fixed pressure levels at 1000, 925, 850, 700, 600, 500, 400, 300, 250, 200, 150, 100, 70, 50, 30, 20, 10, 5, and 1 hPa. Daily outputs of 6 variables have been interpolated to 8 fixed pressure levels at 1000, 850, 700, 500, 250, 100, 50, and 10 hPa.

Output name	Description	Frequency
ta	Air temperature	Monthly/Daily
ua	Eastward wind	Monthly/Daily
va	Northward wind	Monthly/Daily
hus	Specific humidity	Monthly/Daily
hur	Relative humidity	Monthly/Daily
wap	Omega (=dp/dt)	Monthly/Daily
zg	Geopotential height	Monthly
o3	O_3 volume mixing ratio	Monthly
co2	CO_2 volume mixing ratio	Monthly
ch4	CH_4 volume mixing ratio	Monthly
n2o	N_2O volume mixing ratio	Monthly

Data availability statement

The data for the BCC-ESM1 simulations (Zhang et al., 2019) are available on the ESGF nodes (https://esgf-node.llnl.gov/projects/cmip6/). The dataset is in Network Common Data Form (NetCDF), version 4.

Disclosure statement

No potential conflicts of interest are reported by the authors.

REFERENCES

Adler, R. F., and Coauthors, 2003: The version-2 Global Precipitation Climatology Project (GPCP) monthly precipitation analysis (1979–present). *Journal of Hydrometeorology*, **4**, 1147–1167, https://doi.org/10.1175/1525-7541(2003)004<1147:TVGPCP>2.0.CO;2.

Allen, R. J., and Coauthors, 2020: Climate and air quality impacts due to mitigation of non-methane near-term climate forcers. *Atmos. Chem. Phys.*, **20**, 9641–9663, https://doi.org/10.5194/acp-20-9641-2020.

Bindoff, N. L., and Coauthors, 2013: Detection and attribution of climate change: From global to regional. *Climate Change 2013*: *The Physical Science Basis. Contribution of Working Group I to the Fifth Assessment Report of the Intergovernmental Panel on Climate Change*, T. F. Stocker et al., Eds., Cambridge University Press, Cambridge, United Kingdom and New York, NY, USA, 867–952.

Collins, W. J., and Coauthors, 2017: AerChemMIP: Quantifying the effects of chemistry and aerosols in CMIP6. *Geoscientific Model Development*, **10**, 585–607, https://doi.org/10.5194/gmd-10-585-2017.

Copernicus Climate Change Service (C3S), 2017: ERA5: Fifth Generation of ECMWF Atmospheric Reanalyses of the Global Climate. Copernicus Climate Change Service Climate Data Store (CDS), Date of Access. [Available online from https://cds.climate.copernicus.eu/cdsapp#!/home]

EANET, 2019: Third periodic report on the state of acid deposition in East Asia. Network Center for the EANET, Niigata, Japan, 43 pp.

Eyring, V., S. Bony, G. A. Meehl, C. A. Senior, B. Stevens, R. J. Stouffer, and K. E. Taylor, 2016: Overview of the Coupled Model Intercomparison Project Phase 6 (CMIP6) experimental design and organization. *Geoscientific Model Development*, **9**, 1937–1958, https://doi.org/10.5194/gmd-9-1937-

2016.

Flynn, C. M., and T. Mauritsen, 2020: On the climate sensitivity and historical warming evolution in recent coupled model ensembles. *Atmospheric Chemistry and Physics*, **20**, 7829–7842, https://doi.org/10.5194/acp-20-7829-2020.

Gregory, J. M., and Coauthors, 2004: A new method for diagnosing radiative forcing and climate sensitivity. *Geophysical Research Letters*, **31**, L03205, https://doi.org/10.1029/2003GL018747.

Griffies, S. M., and Coauthors, 2005: Formulation of an ocean model for global climate simulations. *Ocean Science*, **1**, 45–79, https://doi.org/10.5194/os-1-45-2005.

Griffiths, P. T., and Coauthors, 2020: Tropospheric ozone in CMIP6 Simulations. *Atmospheric Chemistry and Physics*, https://doi.org/10.5194/acp-2019-1216.

Grose, M. R., J. Gregory, R. Colman, and T. Andrews, 2018: What climate sensitivity index is most useful for projections? *Geophys. Res. Lett.*, **45**, 1559–1566, https://doi.org/10.1002/2017GL075742.

Horowitz, L. W., and Coauthors, 2003: A global simulation of tropospheric ozone and related tracers: Description and evaluation of MOZART, version 2. *J. Geophys. Res.*, **108**, 4784, https://doi.org/10.1029/2002jd002853.

Lamarque, J. F., and Coauthors, 2013: The Atmospheric Chemistry and Climate Model Intercomparison Project (ACCMIP): Overview and description of models, simulations and climate diagnostics. *Geoscientific Model Development*, **6**, 179–206, https://doi.org/10.5194/gmd-6-179-2013.

Li, W. P., Y. W. Zhang, X. L. Shi, W. Y. Zhou, A. N. Huang, M. Q. Mu, B. Qiu, and J. J. Ji, 2019: Development of land surface model BCC_AVIM2.0 and its preliminary performance in LS3MIP/CMIP6. *Journal of Meteorological Research*, **33**, 851–869, https://doi.org/10.1007/s13351-019-9016-y.

Malm, W. C., B. A. Schichtel, M. L. Pitchford, L. L. Ashbaugh, and R. A. Eldred, 2004: Spatial and monthly trends in speciated fine particle concentration in the United States. *J. Geophys. Res.*, **109**, D03306, https://doi.org/10.1029/2003JD003739.

Meehl, G.A., and Coauthors, 2020: Context for interpreting equilibrium climate sensitivity and transient climate response from the CMIP6 Earth system models. *Science Advances*, **6**(26), https://doi.org/10.1126/sciadv.aba1981.

Mulcahy, J. P., and Coauthors, 2020: Description and evaluation of aerosol in UKESM1 and HadGEM3-GC3.1 CMIP6 historical simulations. *Geoscientific Model Development Discussions*, https://doi.org/10.5194/gmd-2019-357.

Oueslati, B., and G. Bellon, 2015: The double ITCZ bias in CMIP5 models: Interaction between SST, large-scale circulation and precipitation. *Climate Dyn.*, **44**, 585–607, https://doi.org/10.1007/s00382-015-2468-6.

Pincus, R., P. M. Forster, and B. Stevens, 2016: The Radiative Forcing Model Intercomparison Project (RFMIP): Experimental protocol for CMIP6. *Geoscientific Model Development*, **9**, 3447–3460, https://doi.org/10.5194/gmd-9-3447-2016.

Schnell, J. L., M. J. Prather, B. Josse, V. Naik, L. W. Horowitz, G. Zeng, D. T. Shindell, and G. Faluvegi, 2016: Effect of climate change on surface ozone over North America, Europe, and East Asia. *Geophys. Res. Lett.*, **43**, 3509–3518, https://doi.org/10.1002/2016GL068060.

Shi, X. L., X. L. Chen, Y. W. Dai, and G. Q. Hu, 2020: Climate sensitivity and feedbacks of BCC-CSM to idealized CO_2 forcing from CMIP5 to CMIP6. *Journal of Meteorological Research*, **34**, 865–878, https://doi.org/10.1007/s13351-020-9204-9.

Thornhill, G. D., and Coauthors, 2020: Effective radiative forcing from emissions of reactive gases and aerosols - a multimodel comparison. *Atmospheric Chemistry and Physics*, https://doi.org/10.5194/acp-2019-1205.

Tørseth, K., and Coauthors, 2012: Introduction to the European Monitoring and Evaluation Programme (EMEP) and observed atmospheric composition change during 1972-2009. *Atmospheric Chemistry and Physics*, **12**, 5447–5481, https://doi.org/10.5194/acp-12-5447-2012.

Turnock, S. T., and Coauthors, 2015: Modelled and observed changes in aerosols and surface solar radiation over Europe between 1960 and 2009. *Atmospheric Chemistry and Physics*, **15**, 9477–9500, https://doi.org/10.5194/acp-15-9477-2015.

Turnock, S. T., and Coauthors, 2020: Historical and future changes in air pollutants from CMIP6 models. *Atmospheric Chemistry and Physics Discussions*, https://doi.org/10.5194/acp-2019-1211.

Winton, M., 2000: A reformulated three-layer sea ice model. *Journal of Atmospheric and Oceanic Technology*, **17**, 525–531, https://doi.org/10.1175/1520-0426(2000)017<0525:ARTLSI>2.0.CO;2.

Wu, T., and Coauthers, 2020b: BCC-CSM2-HR: A High-Resolution Version of the Beijing Climate Center Climate System Model, Geosci. *Model Dev. Discuss.*, https://doi.org/10.5194/gmd-2020-284.

Wu, T. W., and Coauthors, 2013: Global carbon budgets simulated by the Beijing climate center climate system model for the last century. *J. Geophys. Res.*, **118**, 4326–4347, https://doi.org/10.1002/jgrd.50320.

Wu, T. W., and Coauthors, 2019a: The Beijing Climate Center Climate System Model (BCC-CSM): The main progress from CMIP5 to CMIP6. *Geoscientific Model Development*, **12**, 1573–1600, https://doi.org/10.5194/gmd-12-1573-2019.

Wu, T. W., A. X. Hu, F. Gao, J. Zhang, and G. A. Meehl, 2019b: New insights into natural variability and anthropogenic forcing of global/regional climate evolution. *npj Climate and Atmospheric Science*, **2**, 18, https://doi.org/10.1038/s41612-019-0075-7.

Wu, T. W., and Coauthors, 2020a: Beijing Climate Center Earth System Model version 1 (BCC-ESM1): Model description and evaluation of aerosol simulations. *Geoscientific Model Development*, **13**, 977–1005, https://doi.org/10.5194/gmd-13-977-2020.

Zhang, J., and Coauthors, 2019: BCC BCC-ESM1 model output prepared for CMIP6 AerChemMIP. *Earth System Grid Federation*, https://doi.org/10.22033/ESGF/CMIP6.1733.

Zhang, X. X., H. L. Liu, and M. H. Zhang, 2015: Double ITCZ in coupled ocean-atmosphere models: From CMIP3 to CMIP5. *Geophys. Res. Lett.*, **42**, 8651–8659, https://doi.org/10.1002/2015GL065973.